ELSEVIER

Chemical Engineering Journal 83 (2001) 33–38

Chemical Engineering Journal

www.elsevier.com/locate/cej

Short communication

Diffusion in surface-wetting films in a two-phase saturated porous solid characterised by pulsed magnetic field gradient NMR

William M. Holmes, Robin G. Graham, Ken J. Packer*

School of Chemistry, University of Nottingham, University Park, Nottingham NG7 2RD, UK

Received 22 August 1999; received in revised form 14 January 2000; accepted 12 April 2000

Abstract

Pulsed-field-gradient NMR measurements of the one-dimensional probability-density distribution $P_\Delta(X)$ for diffusive displacements of water molecules in times Δ in a water-wet sandstone, saturated with a mixture of dodecane and brine, are presented for water saturations $S_w \leq 0.32$. The distributions show a distinctive shape which is attributed to the distribution of the aqueous phase in thin, locally curved and effectively two-dimensional layers on the pore surface. The data are reproduced well by a simple model in which diffusion is restricted to the surfaces of an isotropic array of infinite planes, with an effective diffusion coefficient $D_2(\Delta)$ which shows a systematic dependence on Δ. This is suggested to arise, in the main, from local curvature of the pore surface. © 2001 Elsevier Science B.V. All rights reserved.

Keywords: NMR; Diffusion; Surface

1. Introduction

The distribution of two immiscible fluid phases within a porous solid is governed, inter alia, by the interfacial tensions between the fluids and between each fluid and the solid. For a strongly water-wet porous solid, saturation with a mixture of aqueous and hydrocarbon phases is expected to result in a physically continuous water phase, always in contact with the solid surface, for all achievable relative saturations [1]. The local thickness and geometry of the aqueous layer will depend upon the detailed spatial variation of the curvature of the solid surface, the interfacial tension between the wetting and non-wetting fluid phases and upon S_w. Transport of water through such films is of importance, for example, in imbibition processes [2].

Except in optically transparent materials, the availability of experimental techniques for the characterisation of wetting films within porous solids and their corresponding transport properties is limited. Nuclear magnetic resonance (NMR) methods have increasingly been applied to the investigation of fluids distributed in porous solids [3] and in this paper we present the results of a preliminary study of diffusion within the aqueous wetting phase of a sample of a water-wet sandstone, saturated with 3% NaCl brine and dodecane in varying proportions. We use the pulsed magnetic field gradient (PFG) ^{1}H NMR method to determine the one-dimensional probability density (the so-called propagator) $P_\Delta(X)$ for displacements X in time Δ [4]. The experimentally determined $P_\Delta(X)$ are compared with those calculated for a simple theoretical model and this comparison provides support for the overall quasi-two-dimensional nature of the diffusion in these films as well as the increasing connectedness of the continuous water film as S_w increases from its lowest, irreducible, value, S_{wi}. At this lowest water saturation, however, evidence is found suggesting that non-uniform film thickness occurs over distance scales accessed by the diffusion measurements and that the effective dimensionality of the diffusive process may, locally, be further reduced [1,5].

2. Experimental

2.1. Sample conditioning

All measurements were made on a cylindrical sample of Fontainebleau sandstone which is that used in our previous work [6,7]. It has a porosity, ϕ, of 25%, a permeability, k, of 2.05 Darcy, is 39 mm in diameter and 52 mm in length. It was contained in a flow cell, which has been used to study the flow of single, two- and three-phase fluids through such

* Corresponding author. Tel.: +44-115-951-3569.
E-mail address: ken.packer@nottingham.ac.uk (K.J. Packer).

1385-8947/01/$ – see front matter © 2001 Elsevier Science B.V. All rights reserved.
PII: S1385-8947(00)00199-6

samples [6]. A pressure of approximately 30 bar is applied to the cylindrical surface of the sample via a close-fitting sleeve pressurised with Fluorinert FC16001, a perfluorinated hydrocarbon. This ensures that fluids, injected by means of constant volume flow-rate pumps (Pharmacia) at the front face of the cylindrical sample, can flow only axially through the sample, emerging at the opposite face and that the ^{1}H NMR signals arise only from the fluids contained within the rock sample. In this paper, fluid flow was used only as a means of establishing the required relative saturations of the aqueous and hydrocarbon phases; all the NMR measurements were made with the fluids stationary.

2.2. NMR measurements

All NMR measurements were made using a GE CSI spectrometer, operating for ^{1}H NMR at 85 MHz with the main magnetic field provided by a 31 cm bore horizontal superconducting magnet (Oxford Instruments) equipped with both field shim coils (Oxford Instruments) and Accustar S150 actively-shielded gradient coils. The latter generate field gradients of up to 0.2 T m^{-1} with rise and fall times of gradient pulses being <100 μs. Because of the possible influence on PFG NMR measurements of diffusion through magnetic field gradients within the sample, which may arise from magnetic susceptibility differences between the rock matrix and the saturating fluids, all measurements were made with the APGSTE modification of the PFG NMR experiment [8]. As long as diffusion during the gradient pulse width, δ, may be neglected and the condition $\Delta \gg \delta$ is satisfied, then the NMR signal, $S_\Delta(q_x)$ (where $q_x = 2\pi\gamma\delta g_x$ and g_x is the magnitude of the field gradient pulse applied in the direction x) is related to the desired propagator, $P_\Delta(X)$, as

$$S_\Delta(q_x) = \int_{-\infty}^{\infty} P_\Delta(X) \exp(2\pi i q_x X)\, \mathrm{d}X \quad (1)$$

where the displacement $X(\Delta) = x(\Delta) - x(0)$. $P_\Delta(X)$ is derived from $S_\Delta(q_x)$ by Fourier transformation with respect to q_x.

Spin–lattice relaxation measurements were made by the inversion-recovery method.

2.3. Discrimination between oil and water phases

In order to determine the diffusive behaviour of the aqueous phase alone, the total NMR signal $S_\Delta(q_x)$ had to be separated into the contributions from the oil and water phases. This was achieved, as before [6] by careful shimming of the spatial homogeneity of the magnetic field. Under properly shimmed conditions the ^{1}H NMR spectrum, obtained by Fourier transformation of the time-varying NMR signal produced by the APGSTE sequence could be deconvoluted into the contributions from the two phases by making use of the known relative chemical shifts of water, CH_2 and CH_3 protons, and the known ratio of signal amplitudes arising from CH_2 and CH_3. S_w was determined from the ratio of the area of the peak assigned as water to the total area of a spectrum acquired under conditions which ensured that effects due to the different NMR relaxation rates (T_1 and T_2) of oil and water protons were negligible.

2.4. Determination of diffusion propagators for the aqueous phase

Typically, $S_\Delta(q_x)$ was determined for a central slice of the sample of thickness 36 mm, using the appropriate slice-selective r.f. pulse. This ensured that any effects arising from proximity to the ends of the sample were kept to a minimum. $S_\Delta(q_x)$ for this slice was then measured for, typically, 32 values of q_x in the range $\pm q_{max}$, symmetrically distributed about zero. By selection of the water NMR

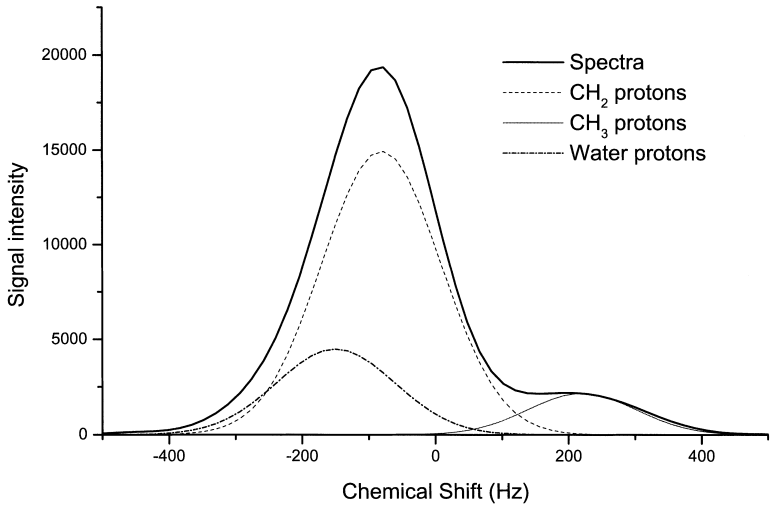

Fig. 1. Typical NMR spectrum of Fontainebleau sandstone with mixed water/oil saturation showing partially resolved water and oil proton signals.

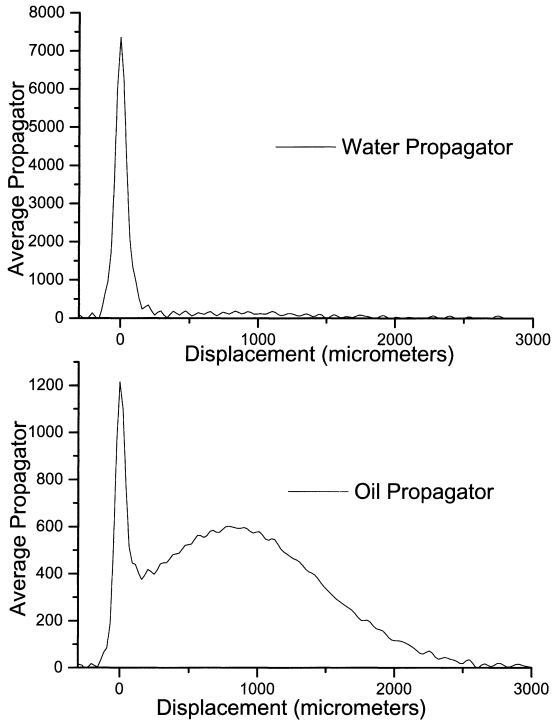

Fig. 2. Resolved water and oil propagators for $S_w = 0.1$ with oil phase flowing at $400\,ml\,h^{-1}$.

signal only, as described above, Fourier transformation of this with respect to q_x then gave the water diffusion propagator $P_{\Delta w}(X)$ at the appropriate S_w. At low values of S_w the question arises as to how well the chemical-shift resolved separation of the water and oil phase signals works, given the large dynamic range of signals involved and the somewhat overlapping nature of the peaks arising from the two phases (see Fig. 1). In order to demonstrate that there was no contribution to the water propagator from the oil signal under conditions of low S_w, the following experiment was performed. Dodecane was pumped through the sample at $400\,ml\,h^{-1}$ which produced a water saturation $S_w = 0.1$. Under the particular conditions of oil flow used, propagators $P_{\Delta}(X)$ for each phase were then measured simultaneously, by the spectral deconvolution described above, and these are shown in Fig. 2. It can be seen that the oil propagator shows the presence of both flowing and non-flowing oil. The fraction which is flowing gives rise to a large Gaussian-like peak with a significant mean displacement. If the deconvolution of the water and oil signals was not fully effective then it would have been expected that the water propagator would have shown such a feature also, particularly as the oil signal is some nine times more intense than that from the water phase under these conditions. However, as can be seen from Fig. 2, the water propagator is symmetrical around zero displacement and shows no detectable contribution which could arise from the overlap of oil signal with that from water. This establishes that the deconvolution is quantitative within the signal-to-noise ratio of the measurements for $S_w = 0.1$.

3. Results and discussion

3.1. Water-wet character of Fontainebleau sandstone

Assuming that the fast diffusion limit applies, the spin–lattice relaxation (SLR) rate R_1 of protons in a fluid in contact with a pore surface of relaxivity ρ is given by [9]

$$R_{1w} = T_{1w}{}^{-1} = \rho\left(\frac{A}{V}\right)_w = \left(\frac{\rho A}{V_0}\right)\left(\frac{1}{S_w}\right) \quad (2)$$

where A and V are the specific surface area and volume, respectively, of the pore space occupied by water with $V = V_0 S_w$ where V_0 is the specific volume of the whole pore space. The SLR for both oil and water phases was single exponential in character. In Fig. 3 we show R_1 plotted as a function of S_w^{-1} for both oil and water protons. It can be seen that the spin–lattice relaxation rate of the oil phase is virtually independent of S_w whereas that for the water protons is close to a linear function of $1/S_w$, consistent with the water phase being present as a surface film, the thickness of which decreases as S_w is reduced. This confirms the strongly water-wet character of the sample.

3.2. Propagators

Propagators for the aqueous phase were measured for relative saturations $S_w = 0.06$, 0.10 and 0.32 at observation times in the range 0.1–1.6 s. In Fig. 4 we compare our measurements at $S_w = 0.06$, $\Delta = 0.8$ s with measurements on the same sample at $S_w = 1$. For $S_w = 1$ the propagator is approximately Gaussian in form indicating that the diffusive process, although restricted, has a three-dimensional character. In striking contrast, the propagator for $S_w = 0.06$ has a pronounced cusp-like form near $X = 0$, and decays much more rapidly than that for $S_w = 1$ with increasing X. This

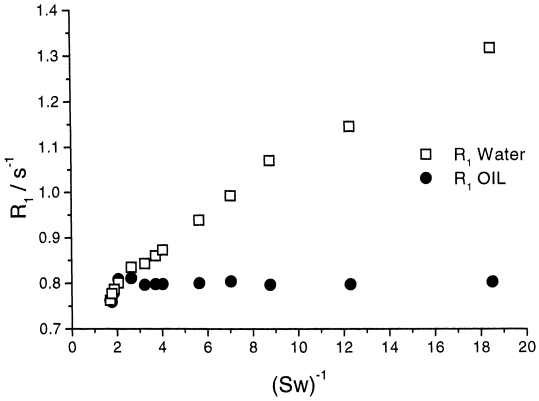

Fig. 3. Spin–lattice relaxation rates for oil and water protons as a function of S_w^{-1}.

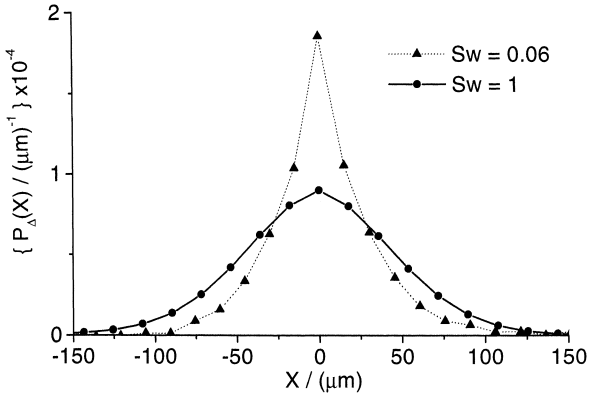

Fig. 4. Water propagators for diffusion measured at $\Delta = 800$ ms for $S_w = 1$ and 0.06.

qualitative difference between the two propagators clearly indicates that the constraints upon diffusive transport, at least in the range of observation times considered here, are quite different in the two cases. The appearance of a cusp-like feature near $X = 0$, is, as we shall now show, characteristic of the powder average of locally two-dimensional propagators and arises, we suggest, from the surface film character of the aqueous phase at low S_w.

Consider a simple model in which the aqueous phase is distributed in thin, uniform films on an istropically oriented array of unconnected planes. Assuming that the film thickness is small compared to the rms displacement in the regime of observation time with which we are concerned, we may, initially, neglect the effects of diffusion across the thickness of the film; for each plane the two-dimensional propagator then takes the form

$$P_\Delta(\xi, \zeta) = \frac{1}{4\pi D_2 \Delta} \exp\left(-\frac{\xi^2 + \zeta^2}{4 D_2 \Delta}\right) \quad (3)$$

where ξ and ζ represent displacements along orthogonal Cartesian axes within the plane and D_2 is the diffusion coefficient on the plane. After projecting Eq. (3) onto the gradient axis and averaging over orientations we find

$$P_\Delta(X) = \sqrt{\frac{\pi}{4 D_2 \Delta}}\, \mathrm{erfc}\left(\sqrt{\frac{X^2}{4 D_2 \Delta}}\right) \quad (4)$$

where erfc is the complementary error function.

In Fig. 5 we show the results of least-squares fits of Eq. (4) to our data for the shortest and longest observation times experimentally accessible, with $D_2(\Delta)$ as an adjustable parameter. Despite its simplicity, the model reproduces the general form of the observed propagators well; in particular, the model propagators show a cusp-like shape near $X = 0$, lending support to our suggestion that this feature in the experimental data arises from locally two-dimensional diffusion. However, if the model were able to account quantitatively for the observed statistics, the parameter D_2 should be independent of Δ and S_w and equal to the self-diffusion coefficient for the bulk fluid. In Fig. 6 we show the least-squares estimates of $D_2(\Delta)$ for all available values of Δ and S_w. It is evident that these estimates depend strongly on both Δ and S_w, two systematic trends being apparent. Firstly, at a given S_w, D_2 decreases, rapidly at first and then less strongly, with

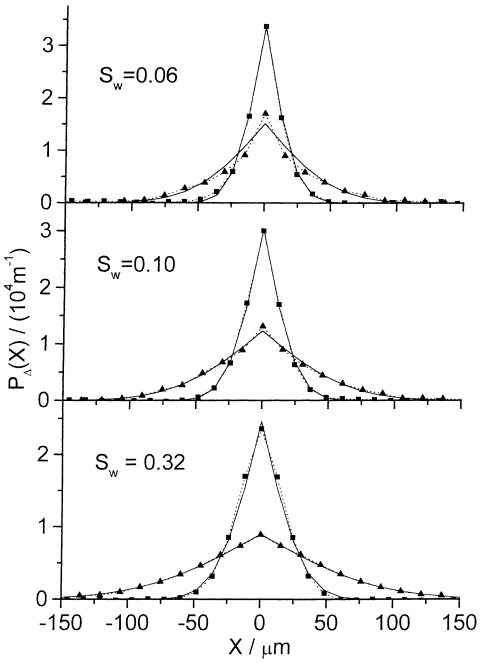

Fig. 5. Least-squares fits (solid lines) of Eq. (4) to experimental propagators measured at $S_w = 0.06$, 10.2 and 0.32 and for times $\Delta = 0.1$ s (squares) and $\Delta = 1.6$ s (triangles). The broken lines connect adjacent data points to aid comparisons.

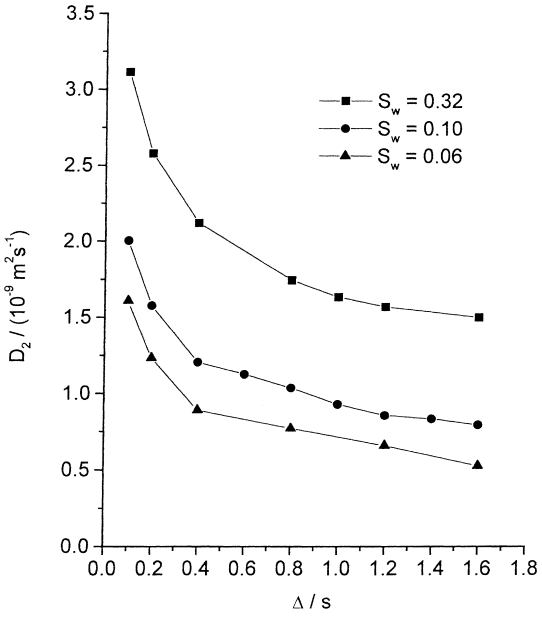

Fig. 6. Dependence of the least-squares estimates of D_2 on Δ obtained by fitting Eq. (4) to propagators measured at $S_w = 0.06$, 0.10 and 0.32. The solid lines joining points are intended only as a guide to the eye.

increasing Δ. Secondly, D_2 increases with increasing S_w, the extent of the increase being nearly independent of Δ.

We first consider the dependence of D_2 upon Δ. It is possible that this behaviour is due to the presence of local curvature in the aqueous films; however it is not obvious that, in the presence of such curvature, the infinite-planes model should be capable of reproducing the detailed form of the observed propagators for any choice of D_2. The general question of how curvature affects the form of the propagator, and hence the results of an attempt to fit the data with the infinite-planes model, is complex and will not be addressed here. Instead, in order to gain some general insight into the problem, we have investigated the effect of curvature by comparing the short-time statistics of particles diffusing on the surface of an isolated sphere, for which analytic results are readily available, with those predicted by the infinite-planes model (at long times, of course, such a comparison becomes meaningless, as the bounded nature of the sphere then dominates the form of the propagator).

For a sphere of radius R the diffusion equation takes the form

$$\frac{\partial P_\Delta^s}{\partial t} = D_s \nabla_s^2 P_\Delta^s \tag{5}$$

where ∇_s^2 is the Laplacian operator on the surface of a sphere. The solution of Eq. (5) is [10]

$$P_\Delta^s(\theta_0, \phi_0, \theta, \phi) = \sum_{k,q} Y_{kq}^*(\theta_0, \phi_0) Y_{kq}(\theta, \phi)\, e^{-\Delta/\tau_k} \tag{6}$$

where (θ_0, ϕ_0), (θ, ϕ) are, respectively, the spherical polar co-ordinates of molecules at $t=0$ and $t=\Delta$, the Y_{kl} are spherical harmonics and

$$\tau_k = \frac{R^2}{k(k+1)D_s} \tag{7}$$

Taking the gradient direction to define the polar axis, we may integrate Eq. (6) over ϕ_0 and ϕ to obtain

$$P_\Delta^s(X) = \frac{1}{4R^2} \int \sum_k (2k+1)\mathcal{P} \times \left(\frac{x_0}{R}\right) \mathcal{P}_k \left(\frac{X+x_0}{R}\right) e^{-\Delta/\tau_k}\, dx_0 \tag{8}$$

where $\mathcal{P}_k$ is the Legendre polynomial of kth degree.

Propagators generated from Eq. (8) and from the infinite-planes model Eq. (4) are compared in Fig. 7, where we have calculated $P_\Delta^s(X)$ from Eq. (8) for a sphere of radius 75 μ with $D_s = 2.2 \times 10^{-9}\ m^2\ s^{-1}$ and $\Delta = 0.1$, 0.8, 1.6 s, then, following the procedure adopted for our experimental data, found the least-squares fit of Eq. (4) to $P_\Delta^s(X)$ with $D_2(\Delta)$ as the fitting parameter. It is evident that for short to intermediate times, when the bounded nature of the isolated-sphere model is relatively insignificant, the infinite-planes model is capable of reproducing (in one dimension at least) the statistics of diffusion on a sphere

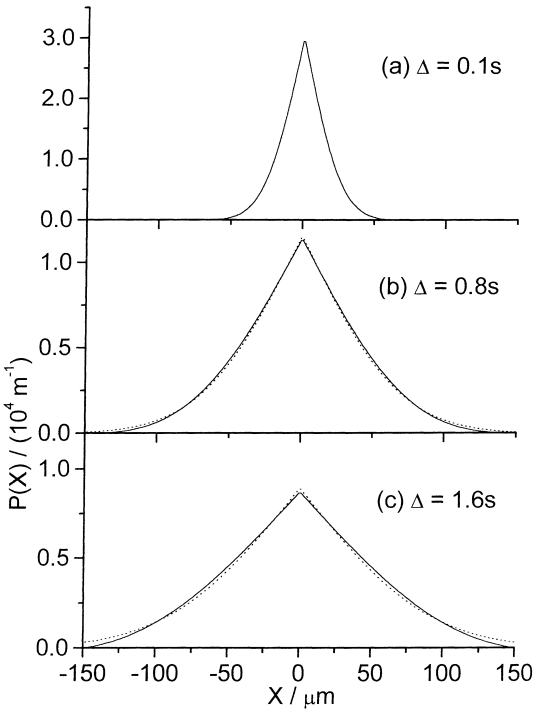

Fig. 7. Fit of infinite planes model (broken lines) to propagators calculated for diffusion on a sphere of radius 75 μm at $\Delta = 0.1$, 0.8 and 1.6 s (solid lines). At $\Delta = 0.1$ s the two curves are indistinguishable at the resolution of the figure.

with near-quantitative accuracy if $D_2(\Delta)$ is regarded as an observation-time dependent quantity. Calculations for a variety of sphere radii and observation times indicate that, for $D_s\Delta/R^2 \leq 0.2$, the dependence of D_2 on observation time and sphere radius is well represented by the equation $D_2(\Delta, R) = D_s(1 - (D_s\Delta/R^2))$.

In the light of this result, we suggest that the rapid initial decrease of D_2 with increasing Δ seen for all values of S_w in Fig. 6 reflects the relatively tight curvature of small-scale irregularities which dominate the statistics at short times. The systematic decrease in the rate at which D_2 falls with increasing Δ may be accounted for by the facts that, as particles explore larger regions of the pore surface, the effects of small-scale irregularities will tend to average to zero, resulting in a larger effective radius of curvature and that the effects of connectivity between differently oriented surfaces will come into play.

We now turn to the dependence of D_2 on S_w. Although, as noted earlier the dependence of D_2 on Δ has a similar form for all three saturations, there is a systematic trend towards higher values of D_2 at a given Δ as S_w increases. In particular, at small Δ, for $S_w = 0.32$ the value of D_2 exceeds the bulk self-diffusion coefficient of water ($\approx 2.2 \times 10^{-9}\ 10\ m^2\ s^{-1}$). This behaviour cannot be interpreted in terms of the curvature of the aqueous film; instead, we believe it arises from a non-negligible contribution to the displacements from diffusion normal to the film surface.

Finally, we make some remarks concerning the quality of fit of the infinite-planes model to the observed propagators (Fig. 5). At the shortest observation time the model reproduces the data with near-quantitative accuracy at all three saturations; however, at longer times there is a systematic tendency to underestimate the probability density near $X = 0$, that tendency increasing with increasing Δ and decreasing with increasing S_w. Although the deviations are small, we believe that they are significant, and we interpret them in the following manner. At low S_w capillary forces will cause a relatively high proportion of the aqueous phase to be held in crevices, which may be locally quasi-one-dimensional or even effectively isolated [1,5]. In either case, we expect a deviation from the infinite-planes model of the type observed, with the deviation becoming more marked with increasing observation time. At higher values of S_w the proportion of water confined to crevices will be smaller, and so, therefore, will the deviations from the model — the propagator now reflects the larger scale structure of the pore and the surface film is smoother, on average.

A second small deviation of a different kind is apparent in the propagator measured at the highest water saturation ($S_w = 0.32$) and small Δ. In this case, the experimental data shows a less pronounced cusp near the origin than predicted by the model. Again, although the deviation is small, we believe it to be significant and attributable to the breakdown of the assumption of negligible film thickness leading to a transition to a more Gaussian-like form for the propagator. This observation is consistent with our explanation of the dependence of D_2 upon S_w.

4. Conclusions

PGSE NMR is able to characterise the diffusive displacement statistics for water molecules in the surface wetting films found in water-wet porous solids at low water saturations. The measured propagator shapes are remarkably well fitted, over the complete range of saturations and observation times investigated, by the simple model of an isotropic superposition of diffusion on infinite planes, as long as the diffusion coefficient is allowed to vary with observation time. It is suggested that this variation of the effective diffusion coefficient arises, in part, from the local curvature of the pore space surfaces and this has been investigated by considering diffusion on the surface of a sphere. Interpretation of the longer time behaviour may well require the consideration of the connectivity and local geometry of the pathways allowing molecules to move from one local curved surface to another differently oriented curved surface. We are currently undertaking more detailed measurements and simulations to extend our understanding of these effects.

Acknowledgements

WMH gratefully acknowledges the award of an EPSRC studentship.

References

[1] J. Bear, Dynamics of Fluids in Porous Media, Elsevier, New York, 1972 (Chapter 9).
[2] M. Sahimi, Flow and Transport in Porous Media and Fractured Rock, VCH, Weinheim, 1995, p. 55.
[3] Proceedings of the Fourth International Meeting on Recent Advances in MR Applications to Porous Media, Trondheim, Norway, 1997, Mag. Reson. Imaging 16 (5/6) (1998).
[4] J. Kärger, W. Heink, J. Mag. Res. 51 (1983) 1.
[5] J.E.M. Snaar, B.P. Hills, Mol. Phys. 86 (1995) 1137.
[6] J.J. Tessier, K.J. Packer, Phys. Fluids 10 (1998) 75.
[7] K.J. Packer, J.J. Tessier, Mol. Phys. 87 (1996) 267.
[8] R.M. Cotts, M.J.R. Hoch, T. Sun, J.T. Marker, J. Mag. Res. 83 (1989) 252.
[9] K.R. Brownstein, C.E. Tarr, Phys. Rev. A19 (1979) 2446.
[10] A. Abragam, The Principles of Nuclear Magnetism, Oxford University Press, Oxford, 1961, p. 298ff.